Ocean Modelling 101 (2016) 113–120

Contents lists available at ScienceDirect

Ocean Modelling

journal homepage: www.elsevier.com/locate/ocemod

Short communication

Conventional versus pre-balanced forms of the shallow-water equations solved using finite-volume method

Xinhua Lu[a,*], Shengbai Xie[b]

[a] State Key Laboratory of Water Resources and Hydropower Engineering Science, Wuhan University, Wuhan 430072, China
[b] College of Ocean, Earth and Environment, University of Delaware, Newark, Delaware 19716, USA

ARTICLE INFO

Article history:
Received 6 July 2015
Revised 26 March 2016
Accepted 8 April 2016
Available online 9 April 2016

Keywords:
FORCE
HLLC
Pre-balanced
Shallow-water equations
SLIC
Well-balanced

ABSTRACT

In the existing literature, various forms of governing equations have been proposed to solve the shallow-water equations (SWEs). Recently, attention has been dedicated to the so-called "pre-balanced" form, because finite-volume schemes that are designed on this basis satisfy the well-balanced property. In this study, we theoretically investigate the relationship between numerical schemes devised using approximate Riemann solvers in the framework of finite-volume methods for solving the conventional form of the SWEs and its "pre-balanced" variant. We find that the numerical schemes for solving these two forms of the SWEs turn out to be identical when some widely employed upwind or centered approximate Riemann solvers are adopted for the numerical flux evaluations, such as the HLL (Harten, Lax, and van Leer), HLLC (HLL solver with restoring the contact surface), FORCE (first-order centered), and SLIC (slope limited centered) schemes. Some numerical experiments are performed, which verify the validity of the result of our theoretical analysis. The theoretical and numerical results suggest that the "pre-balanced" SWEs variant is not superior to the conventional one for solving the SWEs using approximate Riemann solvers.

1. Introduction

In regions where the water depth is far less than the horizontal scale of motion, the shallow-water equations (SWEs) are widely employed for the modelling of flow motions (e.g., flood wave propagation, wave run-ups, wind-induced flow motions), scalar transport (by coupling the SWEs with a scalar transport equation), and sediment transport and the associated morphological processes (by coupling the SWEs with sediment transport and bed deformation equations). In Fig. 1, a sketch of the shallow-water system is presented. The SWEs, in a conservative vector form, can be written as (see, for example, Liang and Borthwick (2009))

$$\frac{\partial \boldsymbol{U}}{\partial t}+\frac{\partial \boldsymbol{F}}{\partial x}+\frac{\partial \boldsymbol{G}}{\partial y}=\boldsymbol{S}, \tag{1}$$

with vectors defined by

$$\boldsymbol{U}=\begin{bmatrix} z \\ q_x \\ q_y \end{bmatrix}, \quad \boldsymbol{F}=\begin{bmatrix} F_c \\ F_x \\ F_y \end{bmatrix}=\begin{bmatrix} q_x \\ F_x \\ uq_y \end{bmatrix},$$

$$\boldsymbol{G}=\begin{bmatrix} G_c \\ G_x \\ G_y \end{bmatrix}=\begin{bmatrix} q_y \\ vq_x \\ G_y \end{bmatrix}, \quad \boldsymbol{S}=\boldsymbol{S}_f+\boldsymbol{S}_0=\begin{bmatrix} 0 \\ S_{fx} \\ S_{fy} \end{bmatrix}+\begin{bmatrix} 0 \\ S_{0x} \\ S_{0y} \end{bmatrix}, \tag{2}$$

where t denotes time; x and y denote the horizontal Cartesian coordinates; z denotes the water surface elevation above a horizontal reference level z_r; h denotes the water depth; and $q_x=uh$ and $q_y=vh$ denote discharges per unit width, with u and v denoting the depth-averaged velocity components in the x- and y-directions, respectively. The terms with subscripts "f" and "0" denote the bed friction and water surface (or bed elevation) gradient related forces, respectively. Throughout this paper, variables in a non-bold style with subscripts "c", "x", and "y", respectively, are related to the continuity equation and the momentum equations in the x- and y-directions, and these variables are the first, second, and third components of a vector. The bed friction force may be calculated using Manning's formula, as

$$S_{fx}=-\frac{gn^2q_x\sqrt{q_x^2+q_y^2}}{h^{7/3}}, \quad S_{fy}=-\frac{gn^2q_y\sqrt{q_x^2+q_y^2}}{h^{7/3}}, \tag{3}$$

where n denotes Manning's roughness coefficient. Note that except z, h could also be used as the conserved variable for the continuity equation (first components of Eqs. (1) and (2)).

Various forms of the SWEs exist in the literature. They mainly differ in the expressions of F_x and S_{0x} in the x-direction and G_y

* Corresponding author at: State Key Laboratory of Water Resources and Hydropower Engineering Science, Wuhan University, Wuhan 430072, China.
E-mail address: xhluhh@whu.edu.cn (X. Lu).

http://dx.doi.org/10.1016/j.ocemod.2016.04.002
1463-5003/

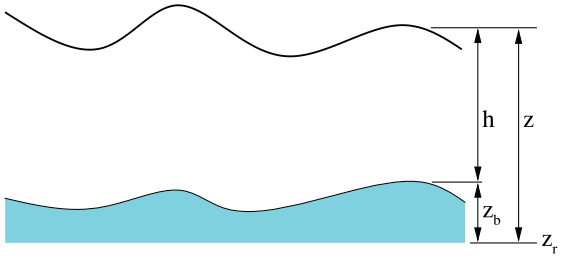

Fig. 1. Sketch of a shallow-water system (not to scale).

and S_{0y} in the y-direction in Eq. (2). For instance, F_x and S_{0x} are commonly written as (Toro, 2001)

$$F_x = uq_x + \frac{1}{2}gh^2, \tag{4a}$$

$$S_{0x} = -gh\frac{\partial z_b}{\partial x}, \tag{4b}$$

where z_b denotes the bed elevation above z_r and physically, z_b satisfies the equality

$$z = h + z_b. \tag{5}$$

For the convenience of descriptions to follow, Eqs. (1) and (2) with F_x and S_{0x} as defined by Eq. (4) will be referred to as the HH form of the SWEs, or simply SWE-HH, in reference to the fact that the expression of F_x (and G_y) contains the term h^2. Other forms of the SWEs can be found in the literature, among which the so-called "pre-balanced" form proposed by Liang and Borthwick (2009) has drawn great attention. Here, a numerical scheme is called well-balanced (e.g., satisfy the C-property) if the discretizations of the flux gradient and source terms in the momentum equations are consistent, such that under a quiescent flow condition over a complex bed topography, no spurious flow is predicted (Bermudez and Vazquez, 1994). Liang and Borthwick (2009) reformulated SWE-HH such that the flux gradient and source terms are perfectly balanced when the HLL (Harten, Lax, and van Leer) approximate Riemann solver (Harten et al., 1983) is used for the numerical flux evaluations. Note that this pre-balanced form of the SWEs was derived specifically for Godunov-type finite-volume schemes, where the relevant expressions of F_x and S_{0x} are defined as

$$F_x = uq_x + \frac{g}{2}z(z - 2z_b), \tag{6a}$$

$$S_{0x} = -gz\frac{\partial z_b}{\partial x}; \tag{6b}$$

the corresponding SWEs will be referred to as the ZZ form of the SWEs, or SWE-ZZ, in viewing of the fact that the expression of F_x (also G_y) contains the term z^2.

Since it was first proposed, the ZZ form of the SWEs has become popular, and has been adopted by many researchers to solve the SWEs over a complex topography (see, for example, Kesserwani and Liang (2010); Huang et al. (2013); Vacondio et al. (2014); Qian et al. (2015)). The idea of pre-balancing by reformulating the HH form of a governing equation system to a ZZ form has been widely adopted to process the flux gradient and source terms in some other equation systems, in which the flux gradient and source terms are the same as those in the SWEs. Such equation systems include the Boussinesq-type equations (Ning et al., 2008), the Green–Naghdi equations (Duran and Marche, 2015; Lannes and Marche, 2015), the SWEs incorporating non-hydrostatic pressure effects (Lu et al., 2015), the two-layer (depth-averaged) shallow-water equations (Cao et al., 2015), and the 3D Reynolds-averaged Navier–Stokes equations in σ coordinates (Ma et al., 2012).

In viewing of the main objective of employing a ZZ form of governing equation systems being to achieve the well-balanced property, and the fact that this property can also be satisfied by numerical schemes devised based on the conventional HH form (see, for example, Zhou et al., (2001); Hou et al. (2013); Hu et al. (2015)), some questions naturally arise. Is it really necessary to use a pre-balanced form of the equation system such as SWE-ZZ instead of SWE-HH, and what is the relation between numerical schemes designed based on different equation system forms? This study aims to address these issues. Note that in this study, we focus our attention on solving the SWEs using finite-volume method (FVM). In particular, we focus on state-of-the-art FVM schemes designed based on the approximate Riemann solvers.

The remainder of this paper is organized as follows. Section 2 presents the FVM discretizations for the SWEs, and revisits the well-balanced property for solving SWE-ZZ. In Section 3, a theoretical analysis is performed to explore the relation between numerical schemes solving the different forms of the SWEs. Finally, conclusions and discussions are presented in Section 4.

2. The well-balancedness of the HLLC-based numerical scheme for solving SWE-ZZ

In this section, we revisit the well-balanced property of SWE-ZZ. In the framework of FVMs, Eq. (1) may be explicitly discretized using the operator-splitting method as (Liang and Borthwick, 2009)

$$\boldsymbol{\varepsilon} = \begin{bmatrix} \varepsilon_c \\ \varepsilon_x \\ \varepsilon_y \end{bmatrix} = \frac{\boldsymbol{U}_{i,j}^{m} - \boldsymbol{U}_{i,j}^{k}}{\Delta t} = \frac{\boldsymbol{F}_{i-1/2,j} - \boldsymbol{F}_{i+1/2,j}}{\Delta x} + \frac{\boldsymbol{G}_{i,j-1/2} - \boldsymbol{G}_{i,j+1/2}}{\Delta y} + (\boldsymbol{S}_0)_{i,j}, \tag{7a}$$

$$\frac{\boldsymbol{U}_{i,j}^{k+1} - \boldsymbol{U}_{i,j}^{m}}{\Delta t} = \boldsymbol{S}_f(\boldsymbol{U}_{i,j}^{k}, \boldsymbol{U}_{i,j}^{k+1}). \tag{7b}$$

Here, i and j denote the cell indexes; Δt and Δx denote the time step and space interval, respectively; "k", "m", and "$k+1$" denote the values at the old, intermediate, and new time levels, respectively; $\boldsymbol{\varepsilon}$ denotes the rate of change of the vector $\boldsymbol{U}$ at the intermediate time level; and $\boldsymbol{F}_{i\pm1/2,j}$ and $\boldsymbol{G}_{i,j\pm1/2}$ are the numerical flux vectors at the cell interfaces. The discretization of the friction force term (see Eq. (7b)) is irrelevant for this study, and the point implicit method (Fiedler and Ramirez, 2000) may be used to enhance numerical stability.

To calculate the numerical fluxes $\boldsymbol{F}_{i\pm1/2,j}$ and $\boldsymbol{G}_{i,j\pm1/2}$ in Eq. (7a), various approaches have been proposed in the literature. Here, we consider a widely used Godunov-type scheme, the HLLC (HLL with restoring the contact surface) approximate Riemann solver (Toro et al., 1994) for flux evaluations. Note that in the original proof of the well-balanced property of SWE-ZZ by Liang and Borthwick (2009), the HLL solver was used. The HLLC solver chosen here is a more sophisticated approach, which will be used in the analysis work in Section 3. Note that if an HLLC-based numerical scheme is well-balanced, then the corresponding HLL-based version should also be well-balanced. The HLL and HLLC solvers rely on evaluations of the eigenstructure of the equation system, and when the eigenstructure of the problem is known they can help resolve sharp fronts in the vicinity of discontinuities with high accuracy, and capture the wet/dry fronts accurately when applied for solving the SWEs (Toro, 2001). The HLLC solver estimates the

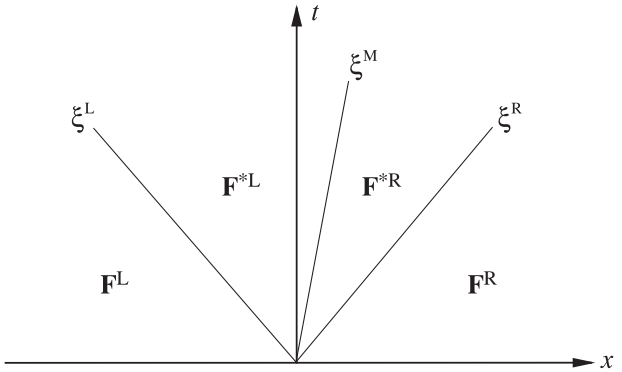

Fig. 2. The solution structure of the HLLC solver.

numerical flux, in the example of the x-direction, as follows:

$$\boldsymbol{F}^{\mathrm{HLLC}}_{i-1/2,j} = \begin{cases} \boldsymbol{F}^{\mathrm{L}}_{i-1/2,j} & \text{if } 0 \leqslant \xi^{\mathrm{L}}_{i-1/2,j}, \quad \text{(a)} \\ \boldsymbol{F}^{*\mathrm{L}}_{i-1/2,j} & \text{if } \xi^{\mathrm{L}}_{i-1/2,j} \leqslant 0 \leqslant \xi^{\mathrm{M}}_{i-1/2,j}, \quad \text{(b)} \\ \boldsymbol{F}^{*\mathrm{R}}_{i-1/2,j} & \text{if } \xi^{\mathrm{M}}_{i-1/2,j} \leqslant 0 \leqslant \xi^{\mathrm{R}}_{i-1/2,j}, \quad \text{(c)} \\ \boldsymbol{F}^{\mathrm{R}}_{i-1/2,j} & \text{if } \xi^{\mathrm{R}}_{i-1/2,j} \leqslant 0 \quad \text{(d).} \end{cases} \tag{8}$$

Here and throughout the remainder of this paper, variables with the superscripts "L", "M", and "R" are related to the left, middle (contact), and right Riemann states at the cell interfaces (see Fig. 2 for the solution structure of the HLLC solver). The superscript "HLLC" indicates that the term or expression is related to the HLLC solver. In Eq. (8), $\boldsymbol{F}^{\mathrm{L}} = \boldsymbol{F}(\boldsymbol{U}^{\mathrm{L}}, z^{\mathrm{L}}_{\mathrm{b}})$, $\boldsymbol{F}^{\mathrm{R}} = \boldsymbol{F}(\boldsymbol{U}^{\mathrm{R}}, z^{\mathrm{R}}_{\mathrm{b}})$, and $\boldsymbol{F}^{*\mathrm{L}}$ and $\boldsymbol{F}^{*\mathrm{R}}$ denote the flux vectors in the middle region. Note that for SWE-HH, $\boldsymbol{F}^{\mathrm{L}}$ is function of $\boldsymbol{U}^{\mathrm{L}}$ and h^{L} (see Eq. (4)), but because z^{L} (the first component of $\boldsymbol{U}^{\mathrm{L}}$), h^{L}, and $z^{\mathrm{L}}_{\mathrm{b}}$ are related (as discussed later in Section 3), we can express $\boldsymbol{F}^{\mathrm{L}}$ as function of $\boldsymbol{U}^{\mathrm{L}}$ and $z^{\mathrm{L}}_{\mathrm{b}}$ for both SWE-HH and SWE-ZZ uniformly. Similarly, $\boldsymbol{F}^{\mathrm{R}}$ can be expressed as function of $\boldsymbol{U}^{\mathrm{R}}$ and $z^{\mathrm{R}}_{\mathrm{b}}$. The variables ξ^{L}, ξ^{M}, and ξ^{R} in Eq. (8) denote wave speeds; in considering the wetting and drying processes, they may be estimated as (Fraccarollo and Toro, 1995)

$$\xi^{\mathrm{L}} = \begin{cases} u^{\mathrm{R}} - 2\sqrt{gh^{\mathrm{R}}}, & \text{if } h^{\mathrm{L}} = 0, \\ \min(u^{\mathrm{L}} - \sqrt{gh^{\mathrm{L}}}, u^{*} - \sqrt{gh^{*}}), & \text{if } h^{\mathrm{L}} > 0, \end{cases} \tag{9a}$$

$$\xi^{\mathrm{R}} = \begin{cases} u^{\mathrm{L}} + 2\sqrt{gh^{\mathrm{L}}}, & \text{if } h^{\mathrm{R}} = 0, \\ \max(u^{\mathrm{R}} + \sqrt{gh^{\mathrm{R}}}, u^{*} + \sqrt{gh^{*}}), & \text{if } h^{\mathrm{R}} > 0, \end{cases} \tag{9b}$$

$$\xi^{\mathrm{M}} = \frac{\xi^{\mathrm{L}} h^{\mathrm{R}}(u^{\mathrm{R}} - \xi^{\mathrm{R}}) - \xi^{\mathrm{R}} h^{\mathrm{L}}(u^{\mathrm{L}} - \xi^{\mathrm{L}})}{h^{\mathrm{R}}(u^{\mathrm{R}} - \xi^{\mathrm{R}}) - h^{\mathrm{L}}(u^{\mathrm{L}} - \xi^{\mathrm{L}})}, \tag{9c}$$

where u^{*} and h^{*} are calculated, respectively, by

$$u^{*} = \frac{1}{2}(u^{\mathrm{L}} + u^{\mathrm{R}}) + \sqrt{gh^{\mathrm{L}}} - \sqrt{gh^{\mathrm{R}}}, \tag{10}$$

and

$$h^{*} = \frac{1}{g}\left[\frac{1}{2}(\sqrt{gh^{\mathrm{L}}} + \sqrt{gh^{\mathrm{R}}}) + \frac{1}{4}(u^{\mathrm{L}} - u^{\mathrm{R}})\right]^2. \tag{11}$$

Note that SWE-HH and SWE-ZZ have the same eigenstructure (Toro, 2001; Liang and Borthwick, 2009), and hence they yield identical wave speeds.

The fluxes in the middle region, $\boldsymbol{F}^{*\mathrm{L}}$ and $\boldsymbol{F}^{*\mathrm{R}}$ in Eq. (8), are computed by

$$\boldsymbol{F}^{*\mathrm{L}} = \begin{bmatrix} F^{*}_1 \\ F^{*}_2 \\ v^{\mathrm{L}} F^{*}_1 \end{bmatrix}, \quad \boldsymbol{F}^{*\mathrm{R}} = \begin{bmatrix} F^{*}_1 \\ F^{*}_2 \\ v^{\mathrm{R}} F^{*}_1 \end{bmatrix}, \tag{12}$$

where $\boldsymbol{F}^{*} = [F^{*}_1\ F^{*}_2\ F^{*}_3]^{\mathrm{tr}}$ (here "tr" denotes transpose of a matrix) is estimated using the classical HLL formula as (Harten et al., 1983)

$$\boldsymbol{F}^{*} = \frac{\xi^{\mathrm{R}}\boldsymbol{F}^{\mathrm{L}} - \xi^{\mathrm{L}}\boldsymbol{F}^{\mathrm{R}} + \xi^{\mathrm{L}}\xi^{\mathrm{R}}(\boldsymbol{U}^{\mathrm{R}} - \boldsymbol{U}^{\mathrm{L}})}{\xi^{\mathrm{R}} - \xi^{\mathrm{L}}}. \tag{13}$$

The numerical fluxes in the y-direction can be calculated similarly to those in the x-direction.

In the following, we state some remarks regarding the HLLC flux evaluation method:

1. In the literature, the water depth h and the water surface elevation z can both be used as the conserved variable for the continuity equation. We can prove that the HLLC scheme predicts same solutions of h and z for both forms of the SWEs, whether h or z is used as the conserved variable. A mathematical proof for this will be presented in Section 3.
2. From Eqs. (8) and (12), it is clear that in evaluating the first (and second) component of the numerical flux vector $\boldsymbol{F}^{\mathrm{HLLC}}_{i-1/2,j}$, Eqs. (8)(b) and (8)(c) are identical, and can both be evaluated by the classical HLL formula defined by Eq. (13). This is also the case when evaluating the first and third components of $\boldsymbol{G}^{\mathrm{HLLC}}_{i,j-1/2}$. This remark is valid for solving both SWE-HH and SWE-ZZ.
3. From Remark 1 and Eq. (12), it is clear that the third component of $\boldsymbol{F}^{\mathrm{HLLC}}_{i-1/2,j}$ is the same when solving SWE-HH and SWE-ZZ. Therefore, in solving either of the considered forms of the SWEs, only the second component of $\boldsymbol{F}^{\mathrm{HLLC}}_{i-1/2,j}$ is calculated differently. Similarly, in the y-direction the first two components of $\boldsymbol{G}^{\mathrm{HLLC}}_{i,j-1/2}$ are the same for solving both forms of the SWEs, and only the third component is evaluated differently.

The source terms in the momentum equations for SWE-ZZ are discretized using a central difference scheme, for instance, in the x-direction we have

$$(S_{0x})_{i,j} = -g\frac{z^{\mathrm{R}}_{i-1/2,j} + z^{\mathrm{L}}_{i+1/2,j}}{2}\frac{(z_{\mathrm{b}})^{\mathrm{L}}_{i+1/2,j} - (z_{\mathrm{b}})^{\mathrm{R}}_{i-1/2,j}}{\Delta x}. \tag{14}$$

It is trivial to prove that the numerical scheme for solving SWE-ZZ with the source term discretized using Eq. (14) is well-balanced when the HLLC solver is used for the flux evaluation. The original proof (for the HLL-based numerical scheme) was provided by Liang and Borthwick (2009). We briefly revisit their proof here, and extend it to the HLLC-based numerical scheme. Under a quiescent flow condition with constant water depth $z = \zeta$, the discretized momentum equation in the x-direction (i.e., the second component of Eq. (7a)) reduces to

$$(\varepsilon_x)_{i,j} = \frac{(F_x)^{\mathrm{HLLC}}_{i-1/2,j} - (F_x)^{\mathrm{HLLC}}_{i+1/2,j}}{\Delta x} - g\zeta\left.\frac{\partial z_{\mathrm{b}}}{\partial x}\right|_{i,j}. \tag{15}$$

If a single-valued definition for the inter-cell bed elevation is taken, i.e.,

$$\begin{aligned} (z_{\mathrm{b}})^{\mathrm{L}}_{i-1/2,j} &= (z_{\mathrm{b}})^{\mathrm{R}}_{i-1/2,j} = (z_{\mathrm{b}})_{i-1/2,j}, \\ (z_{\mathrm{b}})^{\mathrm{L}}_{i+1/2,j} &= (z_{\mathrm{b}})^{\mathrm{R}}_{i+1/2,j} = (z_{\mathrm{b}})_{i+1/2,j} \end{aligned} \tag{16}$$

then for all the possible HLLC formulae given by Eq. (8), one expresses the numerical fluxes at the cell interfaces under the quiescent flow condition as

$$\begin{aligned} (F_x)^{\mathrm{HLLC}}_{i-1/2,j} &= \frac{g}{2}\zeta(\zeta - 2(z_{\mathrm{b}})_{i-1/2,j}), \\ (F_x)^{\mathrm{HLLC}}_{i+1/2,j} &= \frac{g}{2}\zeta(\zeta - 2(z_{\mathrm{b}})_{i+1/2,j}). \end{aligned} \tag{17}$$

Substituting Eq. (17) into Eq. (15), one obtains that

$$(\varepsilon_x)_{i,j} = g\zeta\frac{(z_{\mathrm{b}})_{i+1/2,j} - (z_{\mathrm{b}})_{i-1/2,j}}{\Delta x} - g\zeta\left.\frac{\partial z_{\mathrm{b}}}{\partial x}\right|_{i,j}. \tag{18}$$

It is obvious that when Eq. (14) is used for the discretization of the second term on the right-hand side of Eq. (18), one arrives at $\varepsilon_x \equiv 0$ under a quiescent flow condition. From the definition of ε_x given by Eq. (7a), we see that no spurious flow is generated when solving the momentum equation in the x-direction. Similarly, we can prove that no spurious flow is generated when solving the momentum equation in the y-direction (i.e., $\varepsilon_y \equiv 0$). Further, no spurious flow is generated when solving the continuity equation (whether h or z is used as the conserved variable) if the inter-cell bed elevation is single-valued. Therefore, the HLLC-based numerical scheme is well-balanced.

As shown above, in order to ensure the property that SWE-ZZ discretized with FVM schemes are well-balanced, z_b should be assumed to be single-valued at the cell interface (see Eq. (16)), which is a common choice in cases where an approximate Riemann solver is employed (see, for example, Zhou et al., (2001); Audusse et al. (2004); Liang and Borthwick (2009)) and is of significant importance for devising FVM schemes that are conservative and well-balanced. Note that the definition provided by Eq. (16) allows solutions over continuous as well as discontinuous bed topographies, as shown by the numerical results given by, for instance, Zhou et al., (2001) and Liang and Borthwick (2009), and also the numerical test in Appendix B.

3. Relation between the HLLC-based numerical schemes for solving SWE-HH and SWE-ZZ

In this section, we theoretically analyze the relation between the numerical schemes for solving the different forms of the SWEs using the HLLC scheme for the numerical flux evaluations. Note that SWE-ZZ was originally proposed and its well-balancedness was proven under a quiescent flow condition. However, it is more meaningful to explore the relation between the numerical schemes for solving SWE-ZZ and the corresponding conventional form (SWE-HH) under a general condition, which is discussed in this section. For convenience, the superscript "HH" or "ZZ" denotes the HH or ZZ form of the SWEs, and "HLLC" indicates that the HLLC-based numerical scheme is used. For instance, the superscript "HLLC-HH" or "HLLC-ZZ" denotes that the HLLC-based numerical scheme is utilized for solving the HH or ZZ form of the SWEs.

In the derivation below, both SWE-ZZ and SWE-HH are discretized using the method presented in Section 2 (see Eqs. (7)–(13)). To simplify the notation, a uniform grid is used in the following derivation. However, the analysis here can straightforwardly be extended to a nonuniform grid discretization by replacing Δx and Δy, respectively, with Δx_i and Δy_j in the following, where Δx_i and Δy_j denote the i-th and j-th grid intervals in the x- and y-directions, respectively. The source terms for SWE-HH are discretized in a similar manner to those for SWE-ZZ (Zhou et al., (2001); Aureli et al. (2008); Hu et al. (2015)). For instance, in the x-direction we have

$$(S_{0x})_{i,j} = -g\frac{h^{\mathrm{R}}_{i-1/2,j} + h^{\mathrm{L}}_{i+1/2,j}}{2}\frac{(z_b)^{\mathrm{L}}_{i+1/2,j} - (z_b)^{\mathrm{R}}_{i-1/2,j}}{\Delta x}. \tag{19}$$

The discretization of the bed elevation at the cell interface, which is required for the calculations of the numerical fluxes and source terms, is worth discussing. In the framework of FVMs, in addition to the assumption of single-valuedness of z_b at the cell interface expressed by Eq. (16), it is also physically required according to Eq. (5) that

$$z^{\mathrm{L}}_{i-1/2,j} = (z_b)^{\mathrm{L}}_{i-1/2,j} + h^{\mathrm{L}}_{i-1/2,j}, \quad z^{\mathrm{R}}_{i-1/2,j} = (z_b)^{\mathrm{R}}_{i-1/2,j} + h^{\mathrm{R}}_{i-1/2,j}. \tag{20}$$

Some useful relations based on Eqs. (16) and (20) are derived in the following. First, on the left side of a cell interface, the following holds:

$$\begin{aligned}&\frac{g}{2}z^{\mathrm{L}}_{i-1/2,j}\left(z^{\mathrm{L}}_{i-1/2,j} - 2(z_b)^{\mathrm{L}}_{i-1/2,j}\right)\\ &= \frac{g}{2}(h^{\mathrm{L}}_{i-1/2,j} + (z_b)_{i-1/2,j})(h^{\mathrm{L}}_{i-1/2,j} - (z_b)_{i-1/2,j})\\ &= \frac{g}{2}\left[\left(h^{\mathrm{L}}_{i-1/2,j}\right)^2 - (z_b)^2_{i-1/2,j}\right],\end{aligned} \tag{21}$$

and similarly,

$$\frac{g}{2}z^{\mathrm{R}}_{i-1/2,j}\left(z^{\mathrm{R}}_{i-1/2,j} - 2(z_b)^{\mathrm{R}}_{i-1/2,j}\right) = \frac{g}{2}\left[(h^{\mathrm{R}}_{i-1/2,j})^2 - (z_b)^2_{i-1/2,j}\right]. \tag{22}$$

Second, from Eqs. (21) and (22) and the definitions in Eqs. (4a) and (6a), we obtain the following relations for the flux difference at a same cell interface:

$$\left(F^{\mathrm{HH}}_x - F^{\mathrm{ZZ}}_x\right)\Big|^{\mathrm{L}}_{i-1/2,j} = \left(F^{\mathrm{HH}}_x - F^{\mathrm{ZZ}}_x\right)\Big|^{\mathrm{R}}_{i-1/2,j} = \frac{g}{2}(z_b)^2_{i-1/2,j}, \tag{23a}$$

$$\left[(F^{\mathrm{ZZ}}_x)^{\mathrm{R}} - (F^{\mathrm{ZZ}}_x)^{\mathrm{L}}\right]\Big|_{i\pm1/2,j} = \left[(F^{\mathrm{HH}}_x)^{\mathrm{R}} - (F^{\mathrm{HH}}_x)^{\mathrm{L}}\right]\Big|_{i\pm1/2,j}. \tag{23b}$$

Here and in the following, the superscripts are commutative. For example,

$$(F^{\mathrm{HH}}_x)^{\mathrm{L}} = (F^{\mathrm{L}}_x)^{\mathrm{HH}}. \tag{24}$$

Third, from Eqs. (14) and (19), the following relation for the discretized source terms is obtained:

$$(S_{0x})^{\mathrm{HH}}_{i,j} - (S_{0x})^{\mathrm{ZZ}}_{i,j} = \frac{g}{2\Delta x}\left[(z_b)^2_{i+1/2,j} - (z_b)^2_{i-1/2,j}\right]. \tag{25}$$

For the HLLC solver, depending on the magnitude of the local wave speeds, the numerical flux $(F_x)^{\mathrm{HLLC}}_{i-1/2,j}$ or $(G_x)^{\mathrm{HLLC}}_{i,j-1/2}$ at a cell interface can be evaluated using three (rather than four, see Remark 2 in Section 2) possible formulae, described by Eq. (8). Therefore, for the momentum equation in the x-direction, for a 2D discretized cell with four interfaces, there formally exist $3^4 = 81$ possibilities for calculating the net flux into the cell. In the following, a complicated situation is chosen such that the fluxes at the left and right cell interfaces are evaluated via Eq. (13) (remember that Eqs. (8)(b), (8)(c), and (13) give the same predictions for $(F_x)^{\mathrm{HLLC}}_{i-1/2,j}$; see Remark 2 in Section 2). The numerical fluxes at the bottom and top cell interfaces may be evaluated through any of the three possible formulae described by Eq. (8) in the following derivation; regarding all the other situations, a discussion is provided at the end of this section.

We first verify the validity of Remark 1 in Section 2. Namely, the HLLC scheme leads to same solutions of both $h^{k+1}_{i,j}$ and $z^{k+1}_{i,j}$ whether SWE-HH or SWE-ZZ is considered. Note that for the two forms of the SWEs, the continuity equations are the same if the conserved variables are chosen to be the same (i.e., choosing either h or z for both), and in this case the HLLC scheme should, of course, lead to identical solutions to the continuity equations when solving SWE-HH and SWE-ZZ. Then, we explore the situation when different conserved variables are chosen for the two forms of the SWEs. To begin with, let us use ε^h_c and ε^z_c, respectively, to denote the rate of change of the conserved variable (see Eq. (7a)) when h and z are employed as the conserved variable for the continuity equation. If h is employed as the conserved variable, then we have from Eq. (7) that $h^{k+1}_{i,j} = h^k_{i,j} + (\varepsilon^h_c)_{i,j}\Delta t$. One can then compute the water surface elevation at the new time level from $z^{k+1}_{i,j} = h^{k+1}_{i,j} + (z_b)_{i,j} = (h^k_{i,j} + (z_b)_{i,j}) + (\varepsilon^h_c)_{i,j}\Delta t$, and thus $z^{k+1}_{i,j} = z^k_{i,j} + (\varepsilon^h_c)_{i,j}\Delta t$. When z is used as the conserved variable, the water surface elevation at the new time level is directly computed from Eq. (7). Namely, $z^{k+1}_{i,j} = z^k_{i,j} + (\varepsilon^z_c)_{i,j}\Delta t$. As can be observed, to prove that the two forms of the continuity equations lead to identical predictions for both $h^{k+1}_{i,j}$ and $z^{k+1}_{i,j}$, we need only to prove that $\varepsilon^h_c \equiv \varepsilon^z_c$. From Eqs. (16) and (20), we obtain that $h^{\mathrm{L}}_{i-1/2,j} - h^{\mathrm{R}}_{i-1/2,j} = z^{\mathrm{L}}_{i-1/2,j} - z^{\mathrm{R}}_{i-1/2,j}$, and thus the numerical flux F^{HLLC}_c (and

also G_c^{HLLC}) related to the continuity equation, described by Eqs. (8) and (13), is the same whether h or z is employed as the conserved variable for the continuity equation. Therefore, we obtain from Eq. (7) that $\varepsilon_c^h \equiv \varepsilon_c^z$. This completes the proof.

Next, we prove that the HLLC scheme results in same solutions for the momentum equations whether SWE-HH or SWE-ZZ is considered. For the discretized momentum equation (Eq. (7a)), for both SWE-HH and SWE-ZZ, by using Eq. (13) to estimate the numerical fluxes at the left and right cell interfaces, we have

$$\begin{aligned}\Delta x(\varepsilon_x)_{i,j}^{\mathrm{HLLC}} = {} & (G_x)_{i,j-1/2}^{\mathrm{HLLC}} - (G_x)_{i,j+1/2}^{\mathrm{HLLC}} + (S_{0x})_{i,j} \\ & + \left.\frac{\xi^{\mathrm{R}}F_x^{\mathrm{L}} - \xi^{\mathrm{L}}F_x^{\mathrm{R}} + \xi^{\mathrm{L}}\xi^{\mathrm{R}}\left(q_x^{\mathrm{R}} - q_x^{\mathrm{L}}\right)}{\xi^{\mathrm{R}} - \xi^{\mathrm{L}}}\right|_{i-1/2,j} \\ & - \left.\frac{\xi^{\mathrm{R}}F_x^{\mathrm{L}} - \xi^{\mathrm{L}}F_x^{\mathrm{R}} + \xi^{\mathrm{L}}\xi^{\mathrm{R}}\left(q_x^{\mathrm{R}} - q_x^{\mathrm{L}}\right)}{\xi^{\mathrm{R}} - \xi^{\mathrm{L}}}\right|_{i+1/2,j}, \end{aligned} \tag{26}$$

and thus the corresponding difference between the two forms of the SWEs is

$$\begin{aligned}\Delta x\left[(\varepsilon_x)_{i,j}^{\mathrm{HLLC\text{-}HH}} - (\varepsilon_x)_{i,j}^{\mathrm{HLLC\text{-}ZZ}}\right] = {} & (S_{0x})_{i,j}^{\mathrm{HH}} - (S_{0x})_{i,j}^{\mathrm{ZZ}} \\ & + \frac{\xi_{i-1/2,j}^{\mathrm{R}}\left(F_x^{\mathrm{HH}} - F_x^{\mathrm{ZZ}}\right)\big|_{i-1/2,j}^{\mathrm{L}} - \xi_{i-1/2,j}^{\mathrm{L}}\left(F_x^{\mathrm{HH}} - F_x^{\mathrm{ZZ}}\right)\big|_{i-1/2,j}^{\mathrm{R}}}{\xi_{i-1/2,j}^{\mathrm{R}} - \xi_{i-1/2,j}^{\mathrm{L}}} \\ & - \frac{\xi_{i+1/2,j}^{\mathrm{R}}\left(F_x^{\mathrm{HH}} - F_x^{\mathrm{ZZ}}\right)\big|_{i+1/2,j}^{\mathrm{L}} - \xi_{i+1/2,j}^{\mathrm{L}}\left(F_x^{\mathrm{HH}} - F_x^{\mathrm{ZZ}}\right)\big|_{i+1/2,j}^{\mathrm{R}}}{\xi_{i+1/2,j}^{\mathrm{R}} - \xi_{i+1/2,j}^{\mathrm{L}}}. \end{aligned} \tag{27}$$

Note that the terms $(G_x)_{i,j\pm1/2}^{\mathrm{HLLC}}$ vanish in Eq. (27), because the HLLC solver leads to same predictions for $(G_x)_{i,j\pm1/2}^{\mathrm{HLLC}}$ whether SWE-HH or SWE-ZZ is considered (see Remark 3 in Section 2).

Substituting Eq. (23a) into Eq. (27) yields that

$$\begin{aligned}(\varepsilon_x)_{i,j}^{\mathrm{HLLC\text{-}HH}} - (\varepsilon_x)_{i,j}^{\mathrm{HLLC\text{-}ZZ}} = {} & \frac{g}{2\Delta x}\left[(z_{\mathrm{b}})_{i-1/2,j}^2 - (z_{\mathrm{b}})_{i+1/2,j}^2\right] + (S_{0x})_{i,j}^{\mathrm{HH}} \\ & - (S_{0x})_{i,j}^{\mathrm{ZZ}}. \end{aligned} \tag{28}$$

Then, by plugging Eq. (25) into Eq. (28) one finally arrives at

$$(\varepsilon_x)_{i,j}^{\mathrm{HLLC\text{-}HH}} = (\varepsilon_x)_{i,j}^{\mathrm{HLLC\text{-}ZZ}}. \tag{29}$$

Similarly, we can prove that $(\varepsilon_y)_{i,j}^{\mathrm{HLLC\text{-}HH}} = (\varepsilon_y)_{i,j}^{\mathrm{HLLC\text{-}ZZ}}$.

From the analysis above, it is clear that as long as Eqs. (16) and (20) are satisfied, the HLLC-based numerical schemes for solving SWE-HH and SWE-ZZ are identical. It is worth making some remarks regarding the derivation. First, in the derivation, Eq. (8)(b) (or Eq. (8)(c) or Eq. (13)) is used to evaluate the numerical fluxes on both the left and right cell interfaces of the discretized cell. One can readily verify that for all the other situations, the conclusion that the HLLC-HH and HLLC-ZZ are equivalent to each other remains valid (e.g., by formally setting $\xi^{\mathrm{L}} = 0$ or $\xi^{\mathrm{R}} = 0$ in Eqs. (26)–(29) to switch the relevant flux calculations to use Eq. (8)(a) or (8)(d)). Second, the derivation is independent of the face-value reconstruction method. Hence, the derived result (see Eq. (29)) is the same whether a spatially first-order piecewise constant approach (Godunov, 1959), a spatially second-order MUSCL (Monotonic Upstream-centered Scheme for Conservation Laws) piecewise linear approach (van Leer, 1979), or a high-order scheme (e.g., the third-order piecewise parabolic method (Colella and Woodward, 1984)) is used for the reconstruction of the Riemann states at the cell interface. In addition, the wet/dry treatment algorithm (e.g., through a redefinition of the reconstructed face values (Liang and Borthwick, 2009)) does not affect the analytical result. Moreover, Eq. (7a) is of first-order accuracy in time, and the derivation presented in this section is valid for schemes that are of first-order accuracy in time. In practice, the multi-stage Runge–Kutta scheme can be used to achieve higher-order accuracy in time (see, for example, Wang et al. (2011)), and it is trivial to prove that for each Runge–Kutta stage calculation, the HLLC-HH and HLLC-ZZ result in identical predictions. Also, the MUSCL–Hancock method (van Leer, 1995) can be used to achieve second-order accuracy in time, by evaluating the numerical fluxes using the reconstructed face values that are evolved over a half time step; in this case, Eq. (29) is still valid, as can be proven by showing that the temporally evolved face values are identical when solving both forms of the SWEs (see the mathematical proof in Appendix A). In addition, the derivation presented in this section suggests that the HLL schemes for solving both forms of the SWEs are also identical.

4. Conclusions and discussions

In this study, we have theoretically analyzed the relation between the FVM schemes for solving the SWEs in their conventional form (SWE-HH) and their pre-balanced variant (SWE-ZZ). After revisiting the well-balanced property for SWE-ZZ, we have shown that the numerical balance between the flux gradient and the source terms strongly relies on the assumption of the single-valuedness of the bed elevation at the cell interface. Based on this assumption, we found that the HLL(C)-based numerical schemes for solving both forms of the SWEs are identical.

In Appendix A, we implemented a similar theoretical analysis as that given in Section 3, but using the slope limited centered (SLIC) scheme for the numerical flux evaluations. The SLIC scheme requires no information on the eigenstructure of the considered equation system (Toro, 2001), and is therefore feasible for solving problems where the relevant eigenstructure of an equation system does not exist or cannot be explicitly computed (Hu et al., 2015; Castro-Díaz et al., 2011). We demonstrate in Appendix A that the two forms of the SWEs remain identical when the SLIC scheme is used for the numerical flux evaluations. Because the first-order centered (FORCE) scheme (Toro, 2001) represents a version of the SLIC scheme that is accurate to first order in time (without evolving the face values by a half time step), it is easy to verify that both forms of the SWEs are identical when the FORCE scheme is used for the numerical flux evaluations, by following the same procedures given in Appendix A. Similar analyses regarding other flux evaluation methods are left for future studies.

Furthermore, as validations, some numerical experiments have been carried out which are described in Appendix B. There, a 2D dam-break wave propagating over a dry and discontinuous bed topography was simulated using the HLLC (also SLIC) scheme for solving both SWE-HH and SWE-ZZ. It was demonstrated that the HLLC (also SLIC) scheme simulates identical results when solving both forms of the SWEs, which is consistent with the analytical work.

Finally, it is also expected that the conclusion from our equivalence analysis regarding the two forms of the SWEs is valid for other equation systems that contain the same flux gradient and source terms as in the SWEs. That is, the relevant FVM schemes should be identical for solving the HH and ZZ forms of these equations systems, e.g., the Boussinesq-type equations, the Green–Naghdi equations, the SWEs with incorporating non-hydrostatic pressure effects, the two-layer (depth-averaged) shallow-water equations, and the 3D Reynolds-averaged Navier–Stokes equations in σ coordinates.

Acknowledgements

This work was supported in part by National Natural Science Foundation of China (Grant No. 51409195), the Fundamental Research Funds for the Central Universities (Grant No. 2042014kf0068) and by the China Postdoctoral Science Foundation

(Grand No. 2014M550408). We thank the anonymous reviewers for providing helpful comments.

Appendix A. Relation between the SLIC-based numerical schemes for solving SWE-HH and SWE-ZZ

In this section, we examine the relation between the SLIC-based numerical schemes for solving SWE-HH and SWE-ZZ. First, we briefly introduce the SLIC flux evaluation method.

The SLIC scheme involves three steps for computing the inter-cell numerical flux. First, the face values are reconstructed from those at the cell centers using the MUSCL piecewise linear interpolation method (van Leer, 1979). Then, the reconstructed face values are advanced over a half time step according to the MUSCL–Hancock method, as (van Leer, 1995)

$$\overline{\boldsymbol{U}}^{\mathrm{R}}_{i-1/2,j} = \boldsymbol{U}^{\mathrm{R}}_{i-1/2,j} + \Delta\boldsymbol{U}_{i,j}, \tag{A.1a}$$

$$\overline{\boldsymbol{U}}^{\mathrm{L}}_{i+1/2,j} = \boldsymbol{U}^{\mathrm{L}}_{i+1/2,j} + \Delta\boldsymbol{U}_{i,j}, \tag{A.1b}$$

$$\overline{\boldsymbol{U}}^{\mathrm{T}}_{i,j-1/2} = \boldsymbol{U}^{\mathrm{T}}_{i,j-1/2} + \Delta\boldsymbol{U}_{i,j}, \tag{A.1c}$$

$$\overline{\boldsymbol{U}}^{\mathrm{B}}_{i,j+1/2} = \boldsymbol{U}^{\mathrm{B}}_{i,j+1/2} + \Delta\boldsymbol{U}_{i,j}, \tag{A.1d}$$

where $\Delta\boldsymbol{U}_{i,j}$ is computed from

$$\begin{aligned}\frac{1}{\Delta t/2}\Delta\boldsymbol{U}_{i,j} &= \frac{1}{\Delta x}\left[\boldsymbol{F}\left(\boldsymbol{U}^{\mathrm{R}}_{i-1/2,j}, (z_{\mathrm{b}})_{i-1/2,j}\right) - \boldsymbol{F}\left(\boldsymbol{U}^{\mathrm{L}}_{i+1/2,j}, (z_{\mathrm{b}})_{i+1/2,j}\right)\right] \\ &+ \frac{1}{\Delta y}\left[\boldsymbol{G}\left(\boldsymbol{U}^{\mathrm{T}}_{i,j-1/2}, (z_{\mathrm{b}})_{i,j-1/2}\right) - \boldsymbol{G}\left(\boldsymbol{U}^{\mathrm{B}}_{i,j+1/2}, (z_{\mathrm{b}})_{i,j+1/2}\right)\right] \\ &+ (\boldsymbol{S}_0)_{i,j}.\end{aligned} \tag{A.2}$$

From this point on, variables furnished with an overbar denote values being evolved over a half time step. The superscripts "B" and "T" in Eq. (A.2) indicate that those variables are related to the bottom and top sides of the cell interface, respectively. Note that the assumption that z_{b} is single-valued at the cell interface (i.e., Eq. (16)) is automatically adopted in Eq. (A.2). The value of $\boldsymbol{S}_0$ in Eq. (A.2) is calculated using the values prior to evolution over a half time step. It is important to remark that after the face values being temporally evolved, the physical link between z, h, and z_{b} at the cell interface (see Eq. (20)) still needs to be satisfied. For instance, in the x-direction we have

$$\overline{z}^{\mathrm{L}}_{i-1/2,j} = (z_{\mathrm{b}})_{i-1/2,j} + \overline{h}^{\mathrm{L}}_{i-1/2,j}, \quad \overline{z}^{\mathrm{R}}_{i-1/2,j} = (z_{\mathrm{b}})_{i-1/2,j} + \overline{h}^{\mathrm{R}}_{i-1/2,j}. \tag{A.3}$$

The final step of the SLIC scheme is to compute the numerical flux vectors $\boldsymbol{F}^{\mathrm{SLIC}}_{i\pm1/2,j}$ and $\boldsymbol{G}^{\mathrm{SLIC}}_{i,j\pm1/2}$ in Eq. (7a), by averaging the Lax–Wendroff flux $\boldsymbol{F}^{\mathrm{LW}}_{i\pm1/2,j}$ and the Lax–Friedrichs flux $\boldsymbol{F}^{\mathrm{LF}}_{i\pm1/2,j}$ (Toro, 2001). For instance, in the x-direction,

$$\boldsymbol{F}^{\mathrm{SLIC}}_{i-1/2,j} = \frac{1}{2}\left(\boldsymbol{F}^{\mathrm{LW}}_{i-1/2,j} + \boldsymbol{F}^{\mathrm{LF}}_{i-1/2,j}\right), \tag{A.4}$$

where

$$\boldsymbol{F}^{\mathrm{LW}}_{i-1/2,j} = \boldsymbol{F}\left(\boldsymbol{U}^{\mathrm{LW}}_{i-1/2,j}, (z_{\mathrm{b}})_{i-1/2,j}\right), \tag{A.5a}$$

$$\begin{aligned}\boldsymbol{U}^{\mathrm{LW}}_{i-1/2,j} &= \frac{1}{2}\left(\overline{\boldsymbol{U}}^{\mathrm{L}}_{i-1/2,j} + \overline{\boldsymbol{U}}^{\mathrm{R}}_{i-1/2,j}\right) \\ &- \frac{1}{2}\frac{\Delta t}{\Delta x}\left[\boldsymbol{F}\left(\overline{\boldsymbol{U}}^{\mathrm{R}}_{i-1/2,j}, (z_{\mathrm{b}})_{i-1/2,j}\right) - \boldsymbol{F}\left(\overline{\boldsymbol{U}}^{\mathrm{L}}_{i-1/2,j}, (z_{\mathrm{b}})_{i-1/2,j}\right)\right], \\ \boldsymbol{F}^{\mathrm{LF}}_{i-1/2,j} &= \frac{1}{2}\left[\boldsymbol{F}\left(\overline{\boldsymbol{U}}^{\mathrm{L}}_{i-1/2,j}, (z_{\mathrm{b}})_{i-1/2,j}\right) + \boldsymbol{F}\left(\overline{\boldsymbol{U}}^{\mathrm{R}}_{i-1/2,j}, (z_{\mathrm{b}})_{i-1/2,j}\right)\right] \\ &- \frac{1}{2}\frac{\Delta x}{\Delta t}\left(\overline{\boldsymbol{U}}^{\mathrm{R}}_{i-1/2,j} - \overline{\boldsymbol{U}}^{\mathrm{L}}_{i-1/2,j}\right).\end{aligned} \tag{A.5b}$$

To examine the relation between the SLIC-based numerical schemes for solving the different forms of the SWEs, we first prove that the values of the variables that are temporally evolved in these schemes are the same. From Eq. (A.2), by considering the definitions in Eqs. (4a) and (6a) and applying simple algebraic manipulations, we obtain the the following for the second component of $\Delta\boldsymbol{U}$:

$$\begin{aligned}&\frac{1}{\Delta t/2}\left[(\Delta U_x)^{\mathrm{HH}}_{i,j} - (\Delta U_x)^{\mathrm{ZZ}}_{i,j}\right] \\ &= \frac{1}{\Delta x}\left[\left(F^{\mathrm{HH}}_x - F^{\mathrm{ZZ}}_x\right)\Big|^{\mathrm{R}}_{i-1/2,j} - \left(F^{\mathrm{HH}}_x - F^{\mathrm{ZZ}}_x\right)\Big|^{\mathrm{L}}_{i+1/2,j}\right] \\ &+ \left[(S_{0x})^{\mathrm{HH}}_{i,j} - (S_{0x})^{\mathrm{ZZ}}_{i,j}\right].\end{aligned} \tag{A.6}$$

Here, $(F^{\mathrm{HH}}_x)^{\mathrm{L}}$, $(F^{\mathrm{HH}}_x)^{\mathrm{R}}$, $(F^{\mathrm{ZZ}}_x)^{\mathrm{L}}$, and $(F^{\mathrm{ZZ}}_x)^{\mathrm{R}}$ are defined by Eq. (24). Note that $(G^{\mathrm{HH}}_x - G^{\mathrm{ZZ}}_x)|^{\mathrm{T}}_{i,j-1/2}$ and $(G^{\mathrm{HH}}_x - G^{\mathrm{ZZ}}_x)|^{\mathrm{B}}_{i,j+1/2}$ vanish in Eq. (A.6), because G_x is the same for both forms of the SWEs (see Eqs. (1) and (2)).

By substituting Eqs. (23a) and (25), which remain valid when the temporally evolved values are used to calculate them, into Eq. (A.6), we obtain

$$(\Delta U_x)^{\mathrm{HH}}_{i,j} = (\Delta U_x)^{\mathrm{ZZ}}_{i,j}. \tag{A.7}$$

From the definitions in Eqs. (A.1) and (A.2), we know that the temporally evolved face values for the SLIC-based numerical schemes for solving SWE-HH and SWE-ZZ are identical. That is,

$$\begin{aligned}&(\overline{\boldsymbol{U}}^{\mathrm{L}}_{i+1/2,j})^{\mathrm{HH}} = (\overline{\boldsymbol{U}}^{\mathrm{L}}_{i+1/2,j})^{\mathrm{ZZ}}, \quad (\overline{\boldsymbol{U}}^{\mathrm{R}}_{i-1/2,j})^{\mathrm{HH}} = (\overline{\boldsymbol{U}}^{\mathrm{R}}_{i-1/2,j})^{\mathrm{ZZ}}, \\ &(\overline{\boldsymbol{U}}^{\mathrm{B}}_{i,j+1/2})^{\mathrm{HH}} = (\overline{\boldsymbol{U}}^{\mathrm{B}}_{i,j+1/2})^{\mathrm{ZZ}}, \quad (\overline{\boldsymbol{U}}^{\mathrm{T}}_{i,j-1/2})^{\mathrm{HH}} = (\overline{\boldsymbol{U}}^{\mathrm{T}}_{i,j-1/2})^{\mathrm{ZZ}}.\end{aligned} \tag{A.8}$$

Then, in a similar to how the relations given in Eq. (23a) are derived, one obtains

$$\left(\overline{F}^{\mathrm{HH}}_x - \overline{F}^{\mathrm{ZZ}}_x\right)\Big|^{\mathrm{L}}_{i-1/2,j} = \left(\overline{F}^{\mathrm{HH}}_x - \overline{F}^{\mathrm{ZZ}}_x\right)\Big|^{\mathrm{R}}_{i-1/2,j} = \frac{g}{2}(z_{\mathrm{b}})^2_{i-1/2,j}, \tag{A.9a}$$

$$\left[\left(F^{\mathrm{LW}}_x\right)^{\mathrm{HH}} - \left(F^{\mathrm{LW}}_x\right)^{\mathrm{ZZ}}\right]\Big|_{i-1/2,j} = \frac{g}{2}(z_{\mathrm{b}})^2_{i-1/2,j}. \tag{A.9b}$$

Here, $\overline{F}_x$ and F^{LW}_x are the second components of $\overline{\boldsymbol{F}}$ and $\boldsymbol{F}^{\mathrm{LW}}$, respectively, where $\overline{\boldsymbol{F}} = \boldsymbol{F}(\overline{\boldsymbol{U}}, z_{\mathrm{b}})$.

Next, we find the relations regarding the Lax–Wendroff flux (defined by Eq. (A.5a)) and the Lax–Friedrichs flux (defined by Eq. (A.5b)) between the SLIC-based numerical schemes for solving SWE-HH and SWE-ZZ. For the Lax–Wendroff flux, with the definition given in Eq. (A.5b), we use the relation given in Eq. (23b), which remains valid when the temporally evolved values are used for flux calculations, together with Eq. (A.8), to derive the following:

$$\left[(U_x)^{\mathrm{LW}}_{i-1/2,j}\right]^{\mathrm{HH}} = \left[(U_x)^{\mathrm{LW}}_{i-1/2,j}\right]^{\mathrm{ZZ}}. \tag{A.10}$$

Here, U^{LW}_x is the second component of $\boldsymbol{U}^{\mathrm{LW}}$.

From the definition given in Eq. (A.5a) and the relations in Eqs. (A.9b) and (A.10), we obtain the following for the Lax–Wendroff flux:

$$\begin{aligned}&\left[\left(F^{\mathrm{LW}}_x\right)^{\mathrm{HH}} - \left(F^{\mathrm{LW}}_x\right)^{\mathrm{ZZ}}\right]\Big|_{i-1/2,j} - \left[\left(F^{\mathrm{LW}}_x\right)^{\mathrm{HH}} - \left(F^{\mathrm{LW}}_x\right)^{\mathrm{ZZ}}\right]\Big|_{i+1/2,j} \\ &= \frac{g}{2}(z_{\mathrm{b}})^2_{i-1/2,j} - \frac{g}{2}(z_{\mathrm{b}})^2_{i+1/2,j}.\end{aligned} \tag{A.11}$$

Regarding the Lax–Friedrichs flux, we consider its definition given by Eqs. (A.8) together with Eqs. (A.8) and (A.9a), to obtain

$$\begin{aligned}&\left[\left(F^{\mathrm{LF}}_x\right)^{\mathrm{HH}} - \left(F^{\mathrm{LF}}_x\right)^{\mathrm{ZZ}}\right]\Big|_{i\pm1/2,j} \\ &= \frac{1}{2}\left[\left(\overline{F}^{\mathrm{HH}}_x - \overline{F}^{\mathrm{ZZ}}_x\right)\Big|^{\mathrm{L}}_{i\pm1/2} + \left(\overline{F}^{\mathrm{HH}}_x - \overline{F}^{\mathrm{ZZ}}_x\right)\Big|^{\mathrm{R}}_{i\pm1/2}\right] = \frac{g}{2}(z_{\mathrm{b}})^2_{i\pm1/2,j},\end{aligned} \tag{A.12}$$

and hence

$$\left[\left(F_x^{\mathrm{LF}}\right)^{\mathrm{HH}}-\left(F_x^{\mathrm{LF}}\right)^{\mathrm{ZZ}}\right]\Big|_{i-1/2,j}-\left[\left(F_x^{\mathrm{LF}}\right)^{\mathrm{HH}}-\left(F_x^{\mathrm{LF}}\right)^{\mathrm{ZZ}}\right]\Big|_{i+1/2,j}=\frac{g}{2}(z_{\mathrm{b}})^2_{i-1/2,j}-\frac{g}{2}(z_{\mathrm{b}})^2_{i+1/2,j}. \tag{A.13}$$

From Eq. (A.4) and the relations in Eqs. (A.11) and (A.13), we obtain that

$$\left[(F_x^{\mathrm{SLIC}})_{i-1/2,j}-(F_x^{\mathrm{SLIC}})_{i+1/2,j}\right]^{\mathrm{HH}}-\left[(F_x^{\mathrm{SLIC}})_{i-1/2,j}-(F_x^{\mathrm{SLIC}})_{i+1/2,j}\right]^{\mathrm{ZZ}}=\frac{g}{2}(z_{\mathrm{b}})^2_{i-1/2,j}-\frac{g}{2}(z_{\mathrm{b}})^2_{i+1/2,j}. \tag{A.14}$$

Because the temporally evolved face values and G_x are the same for both forms of the SWEs (see Eq. (A.8) and Eqs. (1) and (2)), we obtain from the expressions of the SLIC scheme (i.e., Eqs. (A.4) and (A.5)) that

$$\left[(G_x^{\mathrm{SLIC}})_{i,j-1/2}-(G_x^{\mathrm{SLIC}})_{i,j+1/2}\right]^{\mathrm{HH}}-\left[(G_x^{\mathrm{SLIC}})_{i,j-1/2}-(G_x^{\mathrm{SLIC}})_{i,j+1/2}\right]^{\mathrm{ZZ}}=0. \tag{A.15}$$

By substituting Eqs. (A.14) and (A.15) into Eq. (7a) and considering the relation in Eq. (25), which remains valid when the temporally evolved values are used for the computation, we finally obtain that

$$(\varepsilon_x)^{\mathrm{SLIC-HH}}_{i,j}=(\varepsilon_x)^{\mathrm{SLIC-ZZ}}_{i,j}. \tag{A.16}$$

Here, the superscripts "SLIC-HH" and "SLIC-ZZ" denote the SLIC-based numerical schemes for solving SWE-HH and SWE-ZZ, respectively. Similarly, we can prove that $(\varepsilon_y)^{\mathrm{SLIC-HH}}_{i,j}=(\varepsilon_y)^{\mathrm{SLIC-ZZ}}_{i,j}$. By following the same procedure used to verify the validity of Remark 1 in Section 2, as presented in Section 3, and noting that $\bar{h}^{\mathrm{L}}_{i-1/2,j}-\bar{h}^{\mathrm{R}}_{i-1/2,j}=\bar{z}^{\mathrm{L}}_{i-1/2,j}-\bar{z}^{\mathrm{R}}_{i-1/2,j}$ if the inter-cell bed elevation is defined to be single-valued, one can easily prove that the SLIC scheme results in the same solutions for both $h^{k+1}_{i,j}$ and $z^{k+1}_{i,j}$ in solving both forms of the SWEs, whether h or z is used as the conserved variable for the continuity equation. Therefore, the SLIC-based numerical schemes for solving SWE-HH and SWE-ZZ are identical, as long as Eqs. (16) and (20) are satisfied.

Appendix B. Numerical evidence

In this section, a numerical test is designed for validating the results of our theoretical analysis on the relation between the numerical schemes for solving different forms of the SWEs. Here, we consider a 2D dam-break wave propagating over a frictionless channel with discontinuous bed topography, defined as follows:

$$z_{\mathrm{b}}(x,y)=\begin{cases}8\mathrm{m} & (x,y)\in\Omega,\\ 0 & \text{else.}\end{cases} \tag{B.1}$$

Here, $\Omega=|x-1000|\leqslant 150\mathrm{m}$ and $|y-750|\leqslant 150\mathrm{m}$. Eq. (B.1) defines a square-shaped obstacle centered at $(x,y)=(1000\mathrm{m},750\mathrm{m})$ in the simulation domain. Initially, the flow is at rest, with the water surface elevation given by

$$z(x,y,t=0)=\begin{cases}10\mathrm{m} & x\leqslant 400\mathrm{m},\\ 0 & \text{else.}\end{cases} \tag{B.2}$$

An open boundary condition is imposed at every boundary. That is, all the gradients of the flow variables vanish at the boundaries. This test includes wet/dry transformations and discontinuity in both the water surface and bed topography, and is thus challenge for a numerical simulation and appropriate for thoroughly validating the analytical results derived in this study.

Concerning the numerical models, the Riemann states z, h, q_x, and q_y, at the cell interface are reconstructed using the MUSCL piecewise linear method (van Leer, 1979) with the minmod slope limiter (Roe and Baines, 1982) to prevent numerical instability. The hydrostatic reconstruction approach proposed by Audusse et al. (2004) is applied to ensure that Eqs. (16) and (20) are satisfied, thus achieving the well-balanced property. In the method of Audusse et al. (2004), a single-valued bed elevation at the cell interface, in the x-direction for example, is defined as

$$(z_{\mathrm{b}})_{i-1/2,j}=\max(z^{\mathrm{L}}_{i-1/2,j}-h^{\mathrm{L}}_{i-1/2,j},z^{\mathrm{R}}_{i-1/2,j}-h^{\mathrm{R}}_{i-1/2,j}). \tag{B.3}$$

Then, h and z at the cell interface are recalculated successively according to

$$h^{\mathrm{L}}_{i-1/2,j}=\max\left(0,z^{\mathrm{L}}_{i-1/2,j}-(z_{\mathrm{b}})_{i-1/2,j}\right),\qquad h^{\mathrm{R}}_{i-1/2,j}=\max\left(0,z^{\mathrm{R}}_{i-1/2,j}-(z_{\mathrm{b}})_{i-1/2,j}\right), \tag{B.4}$$

and

$$z^{\mathrm{L}}_{i-1/2,j}=h^{\mathrm{L}}_{i-1/2,j}+(z_{\mathrm{b}})_{i-1/2,j},\qquad z^{\mathrm{R}}_{i-1/2,j}=h^{\mathrm{R}}_{i-1/2,j}+(z_{\mathrm{b}})_{i-1/2,j}. \tag{B.5}$$

It is worth mentioning that the surface-gradient method (SGM) proposed by Zhou et al., (2001) is also a good choice for reconstructing face values that satisfy Eqs. (16) and (20). In the framework of SGM, the variable z_{b} is defined at the cell interface (on a semi-staggered grid), and thus Eq. (20) is automatically satisfied; the face value of water depth is calculated as, for instance, $h^{\mathrm{L}}_{i-1/2,j}=z^{\mathrm{L}}_{i-1/2,j}-(z_{\mathrm{b}})_{i-1/2,j}$, hence Eq. (20) is fulfilled. We choose the hydrostatic reconstruction approach in this study, because we employ a collocated grid system (all variables are stored at the same locations), and this method ensures non-negative water depth solutions (Audusse et al., 2004). At the wet/dry fronts and in the dry area, the bed slope is locally modified such that no spurious flow is generated there (Brufau et al., 2002). Following Hou et al. (2013), in regions with rapid water depth changes and at the wet/dry fronts, the second-order MUSCL reconstruction scheme is degenerated to a first-order piecewise constant scheme, to avoid predicting extreme velocities. Note that because the MUSCL–Hancock approach is employed, the SLIC-based numerical scheme is of second-order accuracy in time. In order to achieve second-order accuracy in time for the HLLC-based numerical scheme, the two-stage second-order Runge–Kutta scheme is utilized.

In the simulations, the computational domain is discretized by a uniform 300 × 300 mesh. A dynamic time step with the Courant–Friedrichs–Lewy (CFL) value (for definition, see, for example, Zhou et al., (2001)) of 0.5 is employed. In Fig. B.1, we illustrate the velocity field and the water depth distribution at two time instances, computed using the HLLC-based numerical scheme for solving SWE-HH. The first sub-figure (Fig. B.1(a)) presents a situation in which the dam-break wave partially inundates the square-shaped obstacle. The second sub-figure (Fig. B.1(b)) demonstrates a situation where the obstacle is fully submerged. From Fig. B.1(a), we can see that the wet/dry fronts are reasonably captured, and no spurious flow is predicted around the bed topography discontinuity area in the dry bed region (i.e., the numerical scheme is well-balanced). As our focus is on verifying the analytical result regarding the equivalence of the numerical schemes, we will not discuss the physical processes of the results in further depth here. In Fig. B.2, we present the time history of the maximum absolute value of the difference in the predicted water surface elevation over the simulation domain in solving SWE-HH and SWE-ZZ using the HLLC (also SLIC) flux evaluation approach. It is clearly seen that the HLLC (or SLIC)-based numerical scheme solving the two forms of the SWEs results in identical predictions, verifying the validity of the analytical result. Note that, owing to machine error, the results in Fig. B.2 slightly deviate from the zero values after the obstacle is partially or completely submerged.

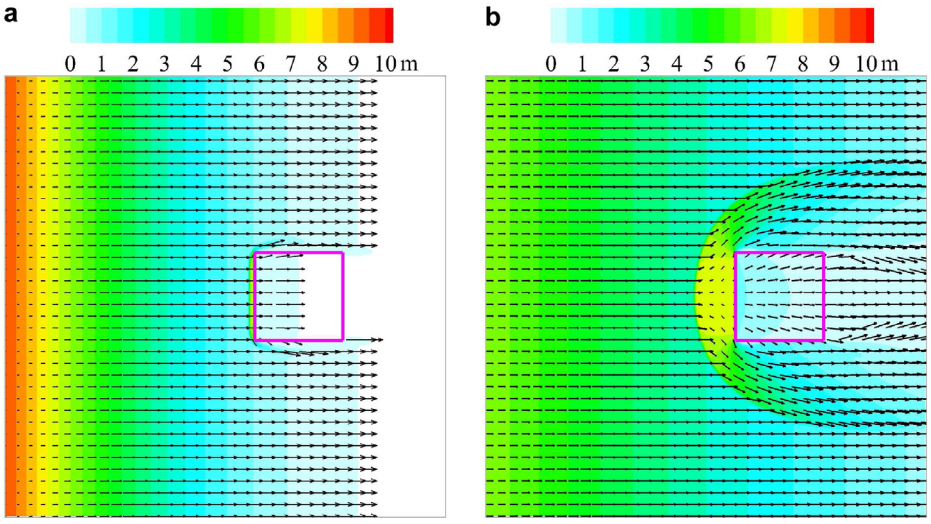

Fig. B.1. Velocity field (vectors) and distribution of water depth (contour) at $t = 42.91$s (a) and $t = 99.13$s (b). The results are computed using the HLLC-based numerical scheme for solving SWE-HH. The vectors are illustrated every 9×9 mesh cell for a clear depiction. The boundary of the simulation domain is indicated by the thin solid lines in gray. The square-shaped obstacle is indicated by the thick solid lines in pink. (For interpretation of the references to colour in this figure legend, the reader is referred to the web version of this article.)

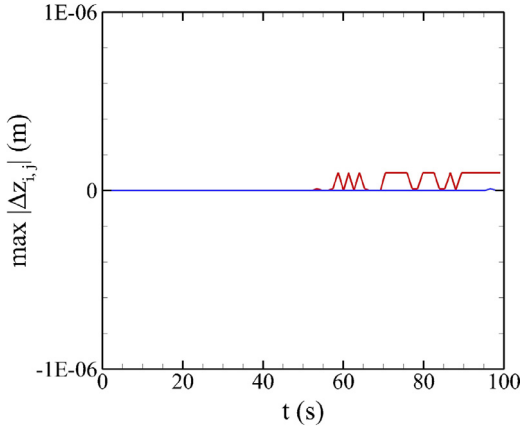

Fig. B.2. Time history of the maximum absolute value of the difference in the predicted water surface elevation in solving SWE-HH and SWE-ZZ using the HLLC (line in red) and SLIC (line in blue) based numerical schemes. (For interpretation of the references to colour in this figure legend, the reader is referred to the web version of this article.)

References

Audusse, E., Bouchut, F., Bristeau, M.-O., Klein, R., Perthame, B., 2004. A fast and stable well-balanced scheme with hydrostatic reconstruction for shallow water flows. SIAM J. Sci. Comput. 25 (6), 2050–2065.

Aureli, F., Maranzoni, A., Mignosa, P., Ziveri, C., 2008. A weighted surface–depth gradient method for the numerical integration of the 2D shallow water equations with topography. Adv. Water. Resour. 31, 962–974.

Bermudez, A., Vazquez, M., 1994. Upwind methods for hyperbolic conservation laws with source terms. Comput. Fluids 23 (8), 1049–1071.

Brufau, P., Vzquez-Cendon, M.E., Garca-Navarro, P., 2002. A numerical model for the flooding and drying of irregular domains. Int. J. Numer. Meth. Fluids 39 (3), 247–275.

Cao, Z., Li, J., Pender, G., Liu, Q., 2015. Whole-process modeling of reservoir turbidity currents by a double layer-averaged model. J. Hydraul. Eng.-ASCE 141, 04014069, 19pp.

Castro-Díaz, M.J., Fernández-Nieto, E.D., González-Vida, J.M., Parés-Madroñal, C., 2011. Numerical treatment of the loss of hyperbolicity of the two-layer shallow-water system. J. Sci. Comput. 48, 16–40.

Colella, P., Woodward, P.R., 1984. The piecewise parabolic method (PPM) for gas-dynamical simulations. J. Comput. Phys. 54, 174–201.

Duran, A., Marche, F., 2015. Discontinuous-Galerkin discretization of a new class of Green–Naghdi equations. Commun. Comput. Phys. 17 (3), 721–760.

Fiedler, F.R., Ramirez, J.A., 2000. A numerical method for simulating discontinuous shallow flow over an infiltrating surface. Int. J. Numer. Meth. Fluids 32, 219–239.

Fraccarollo, L., Toro, E.F., 1995. Experimental and numerical assessment of the shallow water model for two-dimensional dam-break type problems. J. Hydraul. Res. 33 (6), 843–864.

Godunov, S.K., 1959. Finite difference methods for the computation of discontinuous solutions of the equations of fluid dynamics. Matematicheskii Sbornik 47, 271–306.

Harten, A., Lax, P.D., van LeerBram, 1983. On upstream differencing and Godunov–type schemes for hyperbolic conservation laws. SIAM Rev. 25 (1), 35–61.

Hou, J., Liang, Q., Simons, F., Hinkelmann, R., 2013. A stable 2D unstructured shallow flow model for simulations of wetting and drying over rough terrains. Comput. Fluids 82, 132–147.

Hu, P., Li, W., He, Z., Pähtz, T., Yue, Z., 2015. Well-balanced and flexible morphological modeling of swash hydrodynamics and sediment transport. Coast. Eng. 96, 27–37.

Huang, Y., Zhang, N., Pei, Y., 2013. Well-balanced finite volume scheme shallow water flooding and drying over arbitrary topography. Eng. Appl. Comput. Fluid Mech. 7 (1), 40–54.

Kesserwani, G., Liang, Q., 2010. A discontinuous Galerkin algorithm for the two-dimensional shallow water equations. Comput. Methods Appl. Mech. Engrg. 199, 3356–3368.

Lannes, D., Marche, F., 2015. A new class of fully nonlinear and weakly dispersive Green–Naghdi models for efficient 2D simulations. J. Comput. Phys. 282, 238–268.

van Leer, B., 1979. Towards the ultimate conservative difference scheme. V. A second-order sequel to Godunov's method. J. Comput. Phys. 32, 101–136.

van Leer, B., 1995. On the relation between the upwind-differencing schemes of Godunov, Engquist–Osher and Roe. SIAM J. Sci. Comput. 31 (1), 3482–3484.

Liang, Q., Borthwick, A.G.L., 2009. Adaptive quadtree simulation of shallow flows with wet–dry fronts over complex topography. Comput. Fluids 38, 221–234.

Lu, X., Dong, B., Mao, B., Zhang, X., 2015. A two-dimensional depth-integrated non-hydrostatic numerical model for nearshore wave propagation. Ocean Modell. 96, 187–202.

Ma, G., Shi, F., Kirby, J.T., 2012. Shock-capturing non-hydrostatic model for fully dispersive surface wave processes. Ocean. Modell. 43-44, 22–35.

Ning, D.Z., Zang, J., Liang, Q., Taylor, P.H., Borthwick, A.G.L., 2008. Boussinesq cut–cell model for non-linearwave interaction with coastal structures. Int. J. Numer. Meth. Fluids 57, 1459–1483.

Qian, H., Cao, Z., Pender, G., Liu, H., Hu, P., 2015. Well-balanced numerical modelling of non-uniform sediment transport in alluvial rivers. Int. J. Sediment Res. 30 (2), 117–130.

Roe, P.L., Baines, M.J., 1982. Algorithms for advection and shock problems. 4th GAMM Conference on Numerical Methods in Fluid Mechanics, pp. 281–290. Braunschweig, Vieweg.

Toro, E.F., 2001. Shock-capturing methods for free-surface shallow flows. Wiley, Chichester, West Sussex PO19 1UD, England.

Toro, E.F., Spruce, M., Speares, W., 1994. Restoration of the contact surface in the HLL-Riemann solver. Shock Waves 4, 25–34.

Vacondio, R., Dal Palù, A., Mignosa, P., 2014. GPU-enhanced finite volume shallow water solver for fast flood simulations. Environ. Modell. Softw. 57, 60–75.

Wang, Y., Liang, Q., Kesserwani, G., Hall, J.W., 2011. A 2D shallow flow model for practical dam-break simulations. J. Hydraul. Res. 49 (3), 307–316.

Zhou, J.G., Causon, D.M., Mingham, C.G., Ingram, D.M., 2001. The surface gradient method for the treatment of source terms in the shallow-water equations. J. Comput. Phys. 168, 1–25.